Conformational Effects on Tryptophan Fluorescence in Cyclic Hexapeptides

Chia-Pin Pan and Mary D. Barkley
Department of Chemistry, Case Western Reserve University, Cleveland, Ohio

ABSTRACT The peptide bond quenches tryptophan fluorescence by excited-state electron transfer, which probably accounts for most of the variation in fluorescence intensity of peptides and proteins. A series of seven peptides was designed with a single tryptophan, identical amino acid composition, and peptide bond as the only known quenching group. The solution structure and side-chain χ_1 rotamer populations of the peptides were determined by one-dimensional and two-dimensional ^{1}H-NMR. All peptides have a single backbone conformation. The ϕ-, ψ-angles and χ_1 rotamer populations of tryptophan vary with position in the sequence. The peptides have fluorescence emission maxima of 350–355 nm, quantum yields of 0.04–0.24, and triple exponential fluorescence decays with lifetimes of 4.4–6.6, 1.4–3.2, and 0.2–1.0 ns at 5°C. Lifetimes were correlated with ground-state conformers in six peptides by assigning the major lifetime component to the major NMR-determined χ_1 rotamer. In five peptides the $\chi_1 = -60°$ rotamer of tryptophan has lifetimes of 2.7–5.5 ns, depending on local backbone conformation. In one peptide the $\chi_1 = 180°$ rotamer has a 0.5-ns lifetime. This series of small peptides vividly demonstrates the dominant role of peptide bond quenching in tryptophan fluorescence.

INTRODUCTION

The environmental sensitivity of tryptophan fluorescence is reasonably well understood in simple model systems (Callis, 1997; Chen and Barkley, 1998). Ideally, this knowledge could be used to interpret or predict intrinsic protein fluorescence in terms of protein structure around the tryptophan residues. Individual tryptophans in polypeptides often have multiexponential fluorescence decays. Although excited-state reactions are still invoked (Hudson et al., 1999; Ladokhin, 1999; Moncrieffe et al., 2000; Nanda and Brand, 2000), the multiple fluorescence lifetimes are generally attributed to ground-state heterogeneity (Donzel et al., 1974; Dahms et al., 1995; Hellings et al., 2003). The emitting state of the indole chromophore has several nonradiative decay channels, including intersystem crossing (Volkert et al., 1977; Robbins et al., 1980), solvent quenching (McMahon et al., 1992), excited-state proton transfer (Vander Donckt, 1969; Saito et al., 1984; Yu et al., 1992), and excited-state electron transfer (Petrich et al., 1983; Shizuka et al., 1988; Chen et al., 1996; Chen and Barkley, 1998). Neither the ground-state conformations causing the multiple lifetimes nor the quenching mechanisms governing those lifetimes are known for proteins. Recent efforts have focused on the peptide bond as the major quenching group in peptides and proteins (Sillen et al., 2000; Ababou and Bombarda, 2001; Laboulais et al., 2001; Adams et al., 2002; Callis and Vivian, 2003; Hellings et al., 2003). The peptide bond is thought to quench by electron transfer from the excited indole ring (donor) to the carbonyl group (acceptor), forming a *dark radical ion pair* (Callis and Vivian, 2003).

According to transition state theory, the electron transfer rate depends on three factors: driving force of reaction, reorganization energy of solute and surrounding solvent molecules, and electronic coupling matrix between reactant and product states (Marcus and Sutin, 1985). Assuming that the driving force and reorganization energy are invariant and that the electronic coupling matrix decays exponentially with distance between donor and acceptor, the electron transfer rate may be estimated by an exponential function dependent on distance (Hopfield, 1974; McLendon, 1988). Several groups have used distance-dependent electron transfer rates to interpret tryptophan fluorescence lifetimes in peptides (Adams et al., 2002) and proteins (Sillen et al., 2000; Laboulais et al., 2001; Hellings et al., 2003). In contrast, other groups have used the energetic contributions to electron transfer rates to explain tryptophan lifetimes and quantum yields in proteins (Ababou and Bombarda, 2001; Callis and Vivian, 2003). Callis and Vivian (2003) correlated the sum of the driving force and reorganization energy with the average transition energy between the emitting ^1L_a and charge-transfer states. This analysis ignored the distance dependence, because electron transfer between the indole ring and the carbonyl group occurs over short distances (Beratan et al., 1992). Evaluation of different approaches to calculating the electron transfer rate by comparison with experimental data is hampered by the complex quenching environment in proteins.

It would be very helpful to have a model system, in which the local environments of tryptophan are relatively simple, but the fluorescence properties are sufficiently diverse, to test the developing hypotheses about the mechanism of electron transfer. We have been using analogs of the cyclic hexapeptides first studied by Kessler et al. (1988a,b), because the

Submitted December 19, 2003, and accepted for publication January 21, 2004.

Address reprint requests to Dr. Mary D. Barkley, Tel.: 216-368-0602; Fax: 216-368-0604; E-mail: mdb4@case.edu.

© 2004 by the Biophysical Society

0006-3495/04/06/3828/08 $2.00

doi: 10.1529/biophysj.103.038901

cyclic backbone has a single predominant conformation and the side chains are fully exposed to solvent. Our previous study of c[D-PpYTFWF] assigned the three fluorescence lifetimes to the corresponding χ_1 rotamers of the tryptophan side chain by comparing fluorescence decay amplitudes and NMR-determined χ_1 rotamer populations (Adams et al., 2002). We also estimated distance-dependent electron transfer rates and used these values to calculate fluorescence lifetimes for each rotamer, in reasonable agreement with the experimental lifetimes. Rooted in this preliminary success, we designed and synthesized a series of cyclic peptides with the same amino acid composition but with the single tryptophan at different positions in the sequence. This varies the local backbone conformation of the tryptophan residue, which is expected to vary the χ_1 rotamer populations (Dunbrack and Karplus, 1994) as well as the electron transfer rates. Here, we determine the solution structures of the peptides by ^{1}H-NMR and characterize the tryptophan fluorescence by steady-state and time-resolved techniques. Assigning fluorescence lifetimes to χ_1 rotamers yields a set of lifetime values associated with known peptide structures.

MATERIALS AND METHODS

Materials

Oxime resin, *N*-α-*t*-Boc-D-proline, -L-phenylalanine, -L-tryptophan, -L-threonine, 2-(1*H*-benzotriazole-1-yl)-1,1,3,3-tetramethyluronium hexafluorophosphate, and *N*-hydroxybenzotriazole·H_2O were purchased from Novabiochem (San Diego, CA). *N*-α-*t*-Boc-L-phosphotyrosine was purchased from Advanced Chemtech (Louisville, KY). *O*-(7-azabenzotriazol-1-yl)-1,1,3,3-tetramethyluronium hexafluorophosphate was purchased from Perceptive Biosystems (Hamburg, Germany). All other reagents and solvents were highest grade available.

Peptide synthesis

Peptides were synthesized manually by Boc chemistry on oxime resin followed by on-resin cyclization with cleavage as described previously (Adams et al., 2002). Synthesis was started by attaching the following amino acids to the resin: Trp^2, Thr^3, Phe^4, and Phe^6 for c[D-PWTFpYF], Phe^4 for c[D-PWTFFpY], and Phe^5 for c[D-PWTpYFF]; Trp^3 for c[D-PpYWTFF]; Thr^3 for c[D-PpYTWFF] and Phe^3 for c[D-PpYFWFT]; Thr^3 for c[D-PpYTFWF]; and Phe^4 for c[D-PpYTFFW]. Crude products contained ~60–70% cyclic peptide, except for c[D-PWTFpYF]. This sequence gave no major cyclized product, presumably an example of the high sequence dependence of the oxime resin in cyclization (Nishino et al., 1992). Peptides were purified by RP-HPLC on a Vydac C-18 semiprep column (Grace Vydac, Columbia, MD): mobile phase A, CH_3CN; mobile phase B, 22% CH_3OH/H_2O with 0.1% trifluoroacetic acid; gradient A/B, 25–50% at 3 mL/min. Retention times were usually 10–13 min for cyclic peptides. Eluted peptides were lyophilized, and molecular weights were verified by negative-ion electrospray ionization mass spectrometry (MicroMass Quattro II) in the Cleveland Mass Spectrometry Facility, Cleveland State University. All cyclic peptides showed a single peak at m/z 920 (M–H). Peptide purity was estimated to be >99%.

^{1}H-NMR

Solution structures of cyclic peptides were determined at 5°C using a Varian Inova 600 MHz spectrometer (Palo Alto, CA). For experiments in H_2O, 1 mg of peptide was dissolved in 600 μL of 10% D_2O (Cambridge Isotope, Andover, MA), 5 mM phosphate buffer, and the pH was adjusted to 4.5–6. Chemical shifts were referenced to 3-(trimethylsilyl)-propanate-2,2,3,3-*d*4. For experiments in D_2O, 1 mg of peptide sample was dissolved in 600 μL of D_2O. High-resolution one-dimensional experiments were acquired with spectral width of 8000 Hz and 20,480 or 24,576 data points of 64 transients. The temperature dependence of the chemical shifts δ of amide protons was measured in 5° increments from 5 to 40°C. Temperature coefficients $-d\delta/dT$ were determined from the slope of a plot of chemical shift versus temperature by linear regression.

Total correlation spectroscopy (TOCSY) spectra (Bax and Davis, 1985) were acquired with a mixing time of 80 ms, spectral width of 8000 Hz, and 4096 data points in 256 t_1 increments of 32 transients. Water suppression for TOCSY was performed by low-power irradiation with a presaturation delay pulse of 1.5 s. Nuclear Overhauser effect spectroscopy (NOESY) spectra (Kumar et al., 1980) were acquired with mixing times up to 300 ms and 4096 data points in 256-t_1 increments of 64 transients. Water suppression for NOESY was done with either WATERGATE (Piotto et al., 1992) or WET (Smallcombe et al., 1995) pulse sequences. Interproton distances were calculated from NOESY spectra using the isolated two-spin approximation theory. A reference distance of 2.82 Å from the indole NH to H7 of the indole ring was taken from the crystal structure. Coupling constants were measured from high-resolution one-dimensional spectra. Double-quantum filtered-correlated spectroscopy (DQF-COSY) spectra acquired with a spectral width of 8000 Hz and 8192 data points in 256-t_1 increments of 64 transients were used in cases of overlapping resonances.

NMR data were processed using Felix 2000 (Accelrys, San Diego, CA) on INDY or OCTANE workstations (Silicon Graphics, Mountain View, CA). Convolution difference water deconvolution was used to remove the residual water signal from the spectra. Data were routinely zero-filled to twice the number of data points in both dimensions. Sine-bell squared and sine-bell apodization functions were shifted and used to achieve the best resolution and sensitivity in the D1 and D2 dimensions, respectively. The data were then phase-corrected and baseline-corrected in D1 dimension.

Structure determination was carried out using the *NMR-Refine* module of InsightII 2000 (Accelrys) as before (Adams et al., 2002). Ensembles of 30 structures were generated in the DGII submodule from NOE-derived distance restraints, hydrogen-bond restraints, ^3J dihedral-angle restraints, and six chiral restraints (Havel et al., 1983). The intensities of NOE cross-peaks were grouped as strong (1.8–2.7 Å), medium (1.8–3.3 Å), and weak (1.8–5.0 Å). The hydrogen-bond restraints were defined as O···N distance ranges of 2.6–3.2 Å. The ^3J dihedral-angle restraints were derived from the Karplus equation. The DGII calculation was done using 20,000 steps of simulated annealing and 500 steps of conjugate gradient optimization. Final structures were computed from the average of the ensemble. A 500-step conjugate gradient optimization with all restraints was used to release the conformational distortion of side chains caused by the averaging step.

Fluorescence spectroscopy

Absorption and fluorescence measurements were performed on cyclic peptides in 0.01 M phosphate buffer, pH 6.9 at 5°C. Absorption spectra were measured on a Varian Cary 3E UV-vis spectrophotometer. Fluorescence measurements were made under magic-angle conditions. Samples were excited at 300 nm to avoid excitation of phosphotyrosine. Absorbance of samples was <0.05 at 300 nm. Steady-state fluorescence was measured on a SLM 8000 photon counting spectrofluorometer (SLM, Urbana, IL) in ratio mode with single excitation and emission monochromators set at 4-nm bandpass. Emission spectra $I(\lambda)$ were corrected using correction factors determined with a standard lamp from Optronics (Orlando, FL). Centers of gravity of emission spectra λ_{cg} were calculated from

$$\lambda_{cg} = \Sigma_\lambda \lambda I(\lambda)/\Sigma_\lambda I(\lambda). \quad (1)$$

Fluorescence quantum yields Φ were determined relative to tryptophan (Sigma, St. Louis, MO; recrystallized four times from 70% ethanol) in H_2O using a quantum yield of 0.14 at 25°C (Chen, 1967).

Fluorescence lifetimes were measured by time-correlated single photon counting as described in detail elsewhere (Zawadzki et al., 2003). The excitation source was a Tsunami mode-locked Ti-sapphire laser pumped by a Millennia diode-pumped Nd-YVO_4 laser (Spectra-Physics, Mountain View, CA). Emission wavelength was selected by a monochromator with a 4-nm band pass. The instrumental response is ~80 ps full width at half-maximum. Fluorescence decay data with $\geq 2 \times 10^4$ counts in the peak were acquired from 325 to 400 nm emission wavelength in 5-nm increments. Decay data were stored in 1024 channels of 7.3, 9.8, and 24.4 ps per channel, corresponding to 7.5-, 10-, and 25-ns timescales.

Decay curves were deconvolved using the Beechem global program (Beechem, 1989), assuming a sum of exponentials

$$I(\lambda, t) = \Sigma_i \alpha_i(\lambda) \exp(-t/\tau_i) \quad (2)$$

with relative amplitudes $\alpha_i(\lambda)$ and lifetimes τ_i of component i at wavelength λ. Lifetimes but not amplitudes were constrained to be the same in the global analysis. Goodness of fit was judged by reduced chi-square, χ_r^2, and the autocorrelation function of the weighted residuals. The radiative rate constant was calculated from

$$k_r = \Phi/\bar{\tau}, \quad (3)$$

where $\bar{\tau}$ is the amplitude-weighted lifetime

$$\bar{\tau} = \Sigma_i \alpha_i(\lambda)\tau_i / \Sigma_i \alpha_i(\lambda). \quad (4)$$

Decay-associated emission spectra $I_i(\lambda)$ of component i were calculated from the lifetime data and steady-state emission spectrum as

$$I_i(\lambda) = \alpha_i(\lambda)\tau_i I(\lambda) / \Sigma_i \alpha_i(\lambda). \quad (5)$$

Centers of gravity of decay-associated emission spectra λ_{cgi} were calculated using $I_i(\lambda)$ in Eq. 1.

RESULTS AND DISCUSSION

Peptide design

The salient features of the peptide c[D-PpYTFWF] used in our previous study are (Adams et al., 2002): 1), a single tryptophan; 2), no amino-acid side chains that quench 3-methylindole fluorescence (Chen and Barkley, 1998); and 3), a single predominant backbone conformation. In addition, this peptide scaffold offers a range of ϕ-, ψ-angles at different positions in the sequence. Side chain χ_1 rotamer populations depend on the ϕ-, ψ-angles due to repulsive steric interactions with the peptide backbone (Dunbrack and Karplus, 1993, 1994). Therefore, we surmised that moving the tryptophan to different positions in the sequence would vary the χ_1 rotamer populations. Tryptophan fluorescence decays should respond in at least two ways to changes in local backbone conformation. First, the decay amplitudes should change because of the correlation between amplitude and rotamer population (Adams et al., 2002). Second, the fluorescence lifetimes should change because the electron transfer rates depend on peptide structure. The latter is the subject of a future study.

The peptide sequences are summarized in Table 1. Peptides are named by the position of tryptophan in the amino acid sequence. Peptides 4a and 6 were designed by simply switching tryptophan at position 5 in c[D-PpYTFWF] with phenylalanine at positions 4 and 6. The analogous design of switching tryptophan with phosphotyrosine at position 2 yielded a linear peptide, independent of starting residue. Peptides 2a and 2b with phosphotyrosine at positions 4 and 6 instead of position 5 were synthesized instead. The design of peptide 4b will be discussed later.

Peptide structure

The structure of peptide 5 was determined previously by ^{1}H-NMR spectroscopy at 25°C (Adams et al., 2002). The other peptide structures were determined at 5°C, because the NOESY spectra had better signal/noise at the lower temperature, especially in the NH-Hα region. Chemical shifts were assigned using sequential assignments in NOESY spectra and spin-type assignments in TOCSY spectra. The patterns of NOE cross-peaks in the NH-Hα region of the NOESY spectra depend more on the position in the peptide sequence than on the amino acid present at that position. The $^3J_{NH\text{-}H\alpha}$ coupling constants also show position, but little amino acid, dependence, implying that the global backbone conformation is similar in the series of cyclic peptides. The average structures of the peptides were computed from ensembles of 23–29 structures with no NOE distance restraint violations >0.5 Å. The backbone RMSDs are 0.16–0.30 Å and the all-atom RMSDs are 1.26–2.03 Å, consistent with a single predominant backbone conformation and multiple side-chain conformations in each peptide. The aromatic side chains extend out from the cyclic backbone, whereas the threonine hydroxyl hovers over the center of the backbone ring (Kessler et al., 1988a). Fig. 1 shows the backbone and major χ_1 rotamer of the tryptophan side chain of all the peptides. The peptide backbones superpose best at positions 3 and 6.

As noted previously (Kessler et al., 1988a; Adams et al., 2002), the small temperature dependence of the chemical shifts of Xaa^3- and Xaa^6-NH indicates that two hydrogen bonds form between Xaa^3-CO···NH-Xaa^6 and Xaa^6-CO···NH-Xaa^3 in the cyclic peptides (see Table S1 in Supplementary Material). The two hydrogen bonds between Xaa^3 and Xaa^6 lock the backbone in two tight turn-like structures comprising Xaa^6–D-Pro^1–Xaa^2–Xaa^3 and Xaa^3–Xaa^4–Xaa^5–Xaa^6. Comparing the ϕ-, ψ-angles of the peptides (Table 2) with the characteristic values of turn structures identifies a βII′ turn around D-Pro^1–Xaa^2 in peptides 2b, 3, 4a, 5, and 6 and a βI turn around Xaa^4–Xaa^5 in peptides 2a, 2b, 3, 4b, 5, and 6. Long-distance interresidue NOEs and $^3J_{NH\text{-}H\alpha}$ coupling constants support these assignments.

TABLE 1 Tryptophan backbone conformation in cyclic peptides, 5°C, and predicted χ_1 rotamer populations from backbone-dependent rotamer library

Peptide	Sequence	ϕ, ψ	Predicted population		
			$\chi_1 = -60°$	$\chi_1 = 180°$	$\chi_1 = 60°$
2a	c[D-PWTFFpY]	−70°, −32°	0.62	0.22	0.16
2b	c[D-PWTpYFF]	−70°, −29°	0.62	0.22	0.16
3	c[D-PpYWTFF]	−100°, 164°	0.85	0.08	0.07
4a	c[D-PpYTWFF]	−67°, 5°	0.52	0.01	0.47
4b	c[D-PpYFWFT]	−48°, −48°	0.25	0.71	0.04
5*	c[D-PpYTFWF]	−104°, −46°	0.68	0.32	0
6	c[D-PpYTFFW]	−155°, 139°	0.01	0.75	0.24

*25°C, Adams et al., 2002.

Interresidue NOEs for βII′ turns are observed between Xaa^2-NH and Xaa^3-NH, and for βI turns between Xaa^4-NH and Xaa^5-NH and between Xaa^5-NH and Xaa^6-NH. The broad single NH resonance for Xaa^4 and the $^3J_{NH\text{-}H\alpha} = 7.1$–$8.7$ Hz for Xaa^5 indicate ϕ-angles of $\sim -60°$ and $-90°$, respectively (Wuthrich, 1986; Kessler et al., 1988b).

In similar cyclic hexapeptides, a major backbone conformation with all *trans* peptide bonds and a minor conformation with a *cis* peptide bond was observed for five of seven sequences (Kessler et al., 1988b, 1990). The other two sequences as well as our series of cyclic peptides have all *trans* peptide bonds. Sequence comparisons suggest that D-Pro^1–Xaa^2, where Xaa^2 is an aromatic amino acid, confers a single backbone conformation on the cyclic hexapeptide. In general, moving tryptophan to different positions in the sequence does not change the global backbone conformation dramatically. Overlapping the peptide backbones shows some twisting of the backbone ring, particularly at positions 2 and 3 (Table 2). This might be caused by side-chain repulsion given that four of the six amino acids have bulky aromatic side chains. In peptide 4b, the smaller threonine side chain at position 6 folds further into the center of the cyclic backbone, twisting the backbone at positions 5 and 6.

Tryptophan rotamer populations

The χ_1 rotamer populations were determined using coupling constants measured from high-resolution one-dimensional or DQF-COSY spectra at 5°C. The $^3J_{H\alpha\text{–}H\beta}$ coupling constants of aromatic side chains in the peptides range from 4.0–11.7 Hz, indicating multiple χ_1 rotamer conformations (Tables 3, 4, and see Table S2 in Supplementary Material). The NOESY spectra of all the peptides showed a single set of cross-peaks between Hα and Hβ, consistent with fast averaging of side-chain conformations on the NMR time-scale. The relative populations of the canonical $\chi_1 = \pm 60°$ and 180° rotamers were calculated from the $^3J_{H\alpha\text{–}H\beta}$ coupling constants using the Pachler equations (Pachler, 1963). Stereospecific assignment of the major χ_1 rotamer was made for aromatic side chains with resolved cross-peaks between Hα–Hβ and NH–Hβ. The rotamer populations of tryptophan as well as the conformation of the major rotamer are given in Table 3. The populations for peptide 5 at 5°C are close to the previous values at 25°C (Adams et al., 2002). The rotamer populations are similar in peptides 2a, 2b, and 6 and in peptides 4a and 4b. The major rotamer of tryptophan is the $\chi_1 = -60°$ rotamer in peptides 2a, 2b, 3, 4b, and 5 and the $\chi_1 = 180°$ rotamer in peptide 6. The three χ_1 rotamers are about equally populated in peptide 4a. For comparison, Table 1 shows the predicted populations for the three canonical χ_1 rotamers of tryptophan in the backbone-dependent rotamer library (Dunbrack and Karplus, 1993, 1994). This library is

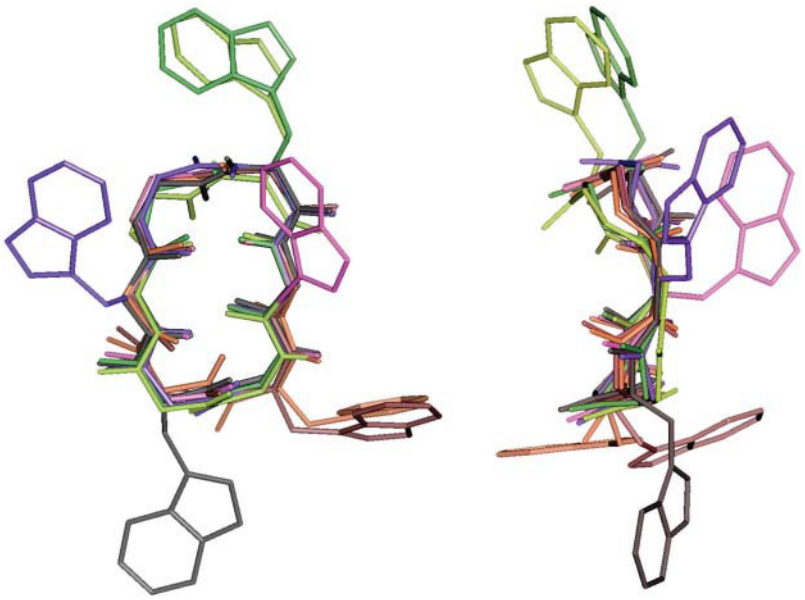

FIGURE 1 Backbones and tryptophan side chains of cyclic hexapeptides 2a (*green*), 2b (*yellow green*), 3 (*magenta*), 4a (*tan*), 4b (*brown*), 5 (*black*), and 6 (*purple*). Backbone HN, N, Cα, and CO atoms superposed best at positions 3 and 6.

TABLE 2 Backbone conformation in cyclic peptides, 5°C

Peptide	D-Pro[1] ϕ, ψ	Xaa[2] ϕ, ψ	Xaa[3] ϕ, ψ	Xaa[4] ϕ, ψ	Xaa[5] ϕ, ψ	Xaa[6] ϕ, ψ
2a	70°, −86°	−70°, −32°	−98°, 162°	−53°, −38°	−78°, −41°	−127°, 85°
2b	65°, −115°	−70°, −29°	−99°, 164°	−52°, −34°	−75°, −53°	−143°, 132°
3	58°, −112°	−65°, −27°	−100°, 164°	−53°, −42°	−73°, −48°	−137°, 124°
4a	75°, −114°	−91°, 54°	−151°, 176°	−67°, 5°	−144°, −58°	−108°, 107°
4b	61°, −94°	−73°, −38°	−94°, 172°	−48°, −48°	−120°, 37°	−154°, 72°
5*	70°, −132°	−87°, 67°	−174°, 156°	−50°, −29°	−104°, −46°	−140°, 123°
6	85°, −109°	−111°, 57°	−149°, 158°	−56°, −23°	−83°, −53°	−155°, 139°

*25°C, Adams et al., 2002.

based on crystal structures of 850 polypeptide chains. Not surprisingly, the predicted and NMR-determined rotamer populations differ somewhat for given ϕ-, ψ-angles, but agree on the major rotamer except in the case of peptide 4b.

For the tryptophan in peptide 4a, the NMR results indicate approximately equal populations of the three χ_1 rotamers, whereas the backbone-dependent rotamer library predicts approximately equal populations of the $\chi_1 = \pm 60°$ rotamers but no $\chi_1 = 180°$ rotamer. Inspection of the structure of peptide 4a reveals that the $\psi = 5°$ backbone conformation results in less steric hindrance for the $\chi_1 = 60°$ rotamer relative to other backbone conformations at position 4 and no steric hindrance by either backbone or adjacent side chains for the $\chi_1 = 180°$ rotamer. In an attempt to increase the population of one tryptophan rotamer, threonine at position 3 was switched with the phenylalanine at position 6 in peptide 4b. Sandwiching tryptophan at position 4 between bulky phenylalanine side chains had only modest effect, although a major $\chi_1 = -60°$ rotamer could be deciphered (Table 4). The $\psi = -48°$ backbone conformation in peptide 4b results in steric repulsion between NH of Phe[5] and the indole side chain for the $\chi_1 = 60°$ rotamer, possibly disfavoring it. On the other hand, the rotamer populations and assignments for other aromatic amino acids in peptides 4a and 4b suggest an explanation for the design failure (Table 4). The major rotamer of Phe[3] in peptide 4b is $\chi_1 = -60°$, so that the phenyl ring points toward pTyr[2] instead of Trp[4] and the expected conformational constraint on Trp[4] fails to occur. The increase in population of the $\chi_1 = -60°$ rotamer of pTyr[2] in peptide 4b, which points the phenol phosphate ring away from Phe[3], is consistent with this explanation. In contrast, the three χ_1 rotamers of Phe[5] are more equally populated, when threonine is placed at position 6.

As in the previous study of peptide 5, the presence of multiple χ_1 rotamers makes it impossible to determine the χ_2 rotamer populations for each χ_1 rotamer. NOE intensities alone can be interpreted at best semiquantitatively. NOE cross-peaks between two Hβ protons and H2 and H4 in the indole ring appear with comparable intensities, suggesting little χ_2 preference for tryptophan in any of the peptides. The presence of cross-peaks between Hα with both H2 and H4, which indicate primarily $(\chi_1, \chi_2) = -60°, -90°; 180°, 90°$ and $(\chi_1, \chi_2) = -60°, 90°; 180°, -90°$, respectively, excludes correlation between χ_1 and χ_2.

TABLE 3 Tryptophan coupling constants and χ_1 rotamer populations in cyclic peptides, 5°C

Peptide	$^3J_{H\alpha-H\beta r}$ (Hz)	$^3J_{H\alpha-H\beta s}$ (Hz)	pI	Major rotamer	pII	pIII
2a	9.1	4.3	0.59	$\chi_1 = -60°$	0.25	0.16
2b	8.8	4.6	0.56	$\chi_1 = -60°$	0.26	0.18
3	4.9	11.7	0.83	$\chi_1 = -60°$	0.21	−0.04
4a	6.4*	5.8*	0.36		0.34	0.30
4b	6.3	7.3	0.43	$\chi_1 = -60°$	0.34	0.23
5	10.4	4.3	0.72	$\chi_1 = -60°$	0.14	0.14
6	8.8	4.0	0.57	$\chi_1 = 180°$	0.30	0.13

*Stereospecificity unresolved.

Fluorescence lifetimes

Fluorescence experiments were performed at 5°C to compare with the NMR data. The absorption spectra of the peptides are identical above 280 nm (data not shown). The slightly higher shoulder at ~270 nm in the peptides compared to tryptophan and *N*-acetyl tryptophanamide (NATA) is likely due to phosphotyrosine. This shoulder is a little different in each peptide. The fluorescence emission maxima vary among the peptides from 350 to 355 nm (Table 5). The wavelength of maximum emission λ_{max} depends on the local

TABLE 4 Coupling constants and χ_1 rotamer populations in c[D-PpYTWFF], 4a, and c[D-PpYFWFT], 4b, 5°C

Residue	$^3J_{H\alpha-H\beta r}$ (Hz)	$^3J_{H\alpha-H\beta s}$ (Hz)	pI	Major rotamer	pII	pIII
		c[D-PpYTWFF], 4a				
D-Pro[1]						
pTyr[2]	10.3	4.3	0.70	$\chi_1 = -60°$	0.16	0.14
Thr[3]						
Trp[4]	6.4*	5.8*	0.36		0.34	0.30
Phe[5]	7.8	6.8	0.47		0.39	0.14
Phe[6]	9.6	4.9	0.64		0.21	0.15
		c[D-PpYFWFT], 4b				
D-Pro[1]						
pTyr[2]	11.3	4.4	0.79	$\chi_1 = -60°$	0.16	0.05
Phe[3]	11.2	5.4	0.79	$\chi_1 = -60°$	0.25	−0.04
Trp[4]	6.3	7.3	0.43	$\chi_1 = -60°$	0.34	0.23
Phe[5]	7.3	5.9	0.43	$\chi_1 = -60°$	0.30	0.27
Thr[6]	3.9					

*Stereospecificity unresolved.

TABLE 5 Fluorescence data, 5°C

Peptide	λ_{max} (nm)	λ_{cg} (nm)	Φ	$\bar{\tau}$ (ns)	$k_r \times 10^{-7}$ (s^{-1})
2a	353	361	0.14 ± 0.01	3.48	4.0 ± 0.3
2b	354	361	0.13 ± 0.01	3.27	4.0 ± 0.3
3	355	361	0.18 ± 0.01	3.28	5.5 ± 0.3
4a	351	360	0.19 ± 0.01	4.58	4.1 ± 0.2
4b	352	360	0.14 ± 0.01	2.84	4.9 ± 0.3
5	350	358	0.24 ± 0.01	4.68	5.1 ± 0.2
6	351	359	0.04 ± 0.002	0.97	4.1 ± 0.2
NATA	353		0.21 ± 0.01	3.83	5.5 ± 0.3

electrostatic environment surrounding the indole ring (Callis and Burgess, 1997; Vivian and Callis, 2001). The small emission spectral shifts reveal subtle differences in electrostatic environment of the solvent-exposed tryptophan in this series of peptides. The fluorescence quantum yields vary sixfold from 0.04 to 0.24. The changes in quantum yield indicate different extents of peptide bond quenching in the peptides.

The fluorescence decays give good fits to four exponential functions (Table 6). The fourth component of ultrashort lifetime τ_4 = 4–90 ps probably represents scattered light. The decay-associated emission spectrum $I_4(\lambda)$ has a Raman peak at 330 nm and decreases monotonically at longer wavelengths (not shown). The maximum contribution at 330 nm corresponds to <0.8% of total intensity for peptides 2a–5 and 1.3% for peptide 6. Recently, a 20-ps component with red-shifted emission spectrum was reported for tryptophan and two peptides (Larsen et al., 2003; Pandit et al., 2003). The decay-associated emission spectra of the 20-ps component include a Raman peak at 320–360 nm and a small broad peak centered around 420 nm. Although our measurements do not extend above 400 nm, $I_4(\lambda)$ of the cyclic peptides showed no signs of increased intensity above 380 nm. The relative amplitudes of the three lifetime components corrected for scattered light are given in Table 6.

As expected, both the relative amplitudes and the lifetimes depend on the peptide. The long lifetime τ_1 ranges from 4.4 to 6.6 ns, the intermediate lifetime τ_2 from 1.4 to 3.2 ns, and the short lifetime τ_3 from 0.2 to 1.0 ns. Four peptides have a salient lifetime component: $\tau_2 = 2.7$ ns of peptide 3, $\tau_1 = 6.6$ ns and $\tau_1 = 5.5$ ns of peptides 4a and 5, and $\tau_3 = 0.5$ ns of peptide 6. The amplitude $\alpha_1 = 0.74$ of peptide 5 at 5°C is somewhat larger than the previous value at 25°C (Adams et al., 2002). In the other three peptides, the major lifetime component appears to be τ_1, although the assignment is less compelling. Two lifetime components, τ_1 and τ_2, have large amplitudes in peptides 2a and 2b, and the three lifetime components have roughly equal amplitudes in peptide 4b. The amplitudes of all peptides show slight wavelength dependence. The centers of gravity of the decay-associated emission spectra $I_i(\lambda)$ are given in Table 6. In five peptides, the λ_{cgi} values of the emission spectra shift progressively to the red with increasing lifetime. However, two peptides do not follow this trend. In peptide 2b, the λ_{cgi} values of the 4.4- and 2.4-ns components are the same and 10 nm to the red of the 1.0-ns component. In peptide 5, the λ_{cgi} values of the 5.5- and 0.8-ns components are red-shifted compared to the 3.2-ns component. If the multiexponential fluorescence decays of the peptides were due to solvent relaxation (Lakowicz, 2000), then all the peptides should show progressively red-shifted decay-associated emission spectra with increasing lifetime. Moreover, solvent relaxation of tryptophan zwitterion has a 1.2-ps decay time in aqueous solution at room temperature (Shen and Knutson, 2001). The relaxation time is unlikely to be three orders-of-magnitude slower for solvent-exposed tryptophans in small peptides.

Radiative rates k_r were calculated from fluorescence quantum yields and amplitude-weighted lifetimes using Eqs. 3 and 4 (Table 5). The values for peptides 3, 4b, and 5 and for NATA are the same within error, whereas the values for peptides 2a, 2b, 4a, and 6 are ~25% lower. An apparent decrease in radiative rate in Pro–Trp and Phe–Trp dipeptides was attributed to intramolecular static quenching (Chen et al., 1991). The ultrafast lifetime component attributed to scattered light could include contributions from statically

TABLE 6 Fluorescence decay parameters, 5°C

Peptide	$\alpha_1(350)$	τ_1 (ns)	λ_{cg1} (nm)	$\alpha_2(350)$	τ_2 (ns)	λ_{cg2} (nm)	$\alpha_3(350)$	τ_3 (ns)	λ_{cg3} (nm)	$\alpha_4(350)$	τ_4 (ns)	λ_{cg4} (nm)	χ_r^2
2a	0.35	4.66	362	0.34	2.76	360	0.07	0.82	352	0.24	0.07	354	1.11
	0.46			0.44			0.10						
2b	0.41	4.39	360	0.29	2.36	360	0.09	1.04	349	0.21	0.08	355	1.05
	0.52			0.37			0.11						
3	0.21	6.03	363	0.48	2.70	359	0.10	0.53	356	0.21	0.06	356	1.08
	0.26			0.61			0.13						
4a	0.20	6.59	361	0.12	2.03	355	0.05	0.19	355	0.63	0.004	355	1.09
	0.55			0.32			0.13						
4b	0.19	5.21	361	0.17	2.04	358	0.14	0.49	355	0.50	0.01	353	1.05
	0.38			0.33			0.29						
5	0.58	5.54	358	0.09	3.20	353	0.10	0.75	357	0.23	0.09	354	1.12
	0.74			0.13			0.13						
6	0.04	4.94	361	0.18	1.38	359	0.45	0.52	357	0.33	0.02	352	1.07
	0.06			0.27			0.67						

Global analysis of data from 325- to 400-nm emission wavelength, 5-nm increments on 7.5-, 10-, and 25-ns timescales. $\Sigma_i \alpha_i(350) = 1$. Second line gives relative amplitudes without scattered light.

quenched species. If so, the fractional intensity of the ultrafast component $f_4 = \alpha_4\tau_4/\Sigma_i\alpha_i\tau_i$ should be higher in peptides evidencing static quenching. However, this trend is not discernable in the data of Table 6.

Correlation of lifetimes and rotamers

The rotamer model of tryptophan photophysics proposes that the multiexponential fluorescence decay represents multiple ground-state conformations (Donzel et al., 1974; Szabo and Rayner, 1980; Ross et al., 1981). Differences among conformers in the local environment of the indole ring presumably cause different fluorescence lifetimes. A number of workers have proposed that the multiple fluorescence lifetimes of single tryptophans in small peptides represent ground-state χ_1 rotamers. For example, the three fluorescence lifetimes of [Trp^2]oxytocin were assigned to canonical χ_1 rotamers of tryptophan by comparing the decay amplitudes with the NMR-determined χ_1 rotamer populations (Ross et al., 1992). Double and triple exponential decays of single tryptophans in α-helix-forming peptides were attributed to χ_1 rotamers (Willis et al., 1994; Clayton and Sawyer, 1999). However, the possibility that multiple backbone conformations also contribute to the lifetime heterogeneity could not be ruled out in these studies. Because each of our cyclic hexapeptides has a single predominant backbone conformation, side-chain rotamers become the only source of conformational heterogeneity. Moreover, the peptide bond is the only known quenching group in the peptides. Therefore, the three fluorescence lifetimes τ_i can be credited to tryptophan rotamers with different excited-state electron transfer rates.

The amplitudes α_i of the fluorescence decay should equal the NMR-determined χ_1 rotamer populations under the following conditions: interconversion of χ_1 rotamers is slow compared to the fluorescence timescale, and χ_2 rotamers do not generate lifetime heterogeneity. This would apply if 1), each χ_1 rotamer has a major χ_2 rotamer; 2), interconversion of χ_2 rotamers is fast compared to the fluorescence timescale (Gordon et al., 1992); or 3), the two canonical χ_2 rotamers of a χ_1 rotamer have the same lifetime. For all peptides except 4a, the α_i value of the major lifetime component (Table 6) is in reasonable agreement with the population pI of the major χ_1 rotamer (Table 3). The small discrepancies between amplitude and rotamer population could be due to experimental error, χ_1 rotamer interconversion on the fluorescence timescale, or χ_2 rotamers. Therefore, we associate the major lifetime component with the corresponding χ_1 rotamer conformation. For peptides 2a, 2b, 3, 4b, and 5, the major lifetime component is assigned to the $\chi_1 = -60°$ rotamer with τ_i values ranging from 2.7 to 5.5 ns. For peptide 6, the major lifetime component is assigned to the $\chi_1 = 180°$ rotamer with $\tau_3 = 0.5$ ns.

The above correlations support the following conclusions. First, the lifetime of a given χ_1 rotamer varies with the conformation of the peptide backbone, resulting from differences in local environment around the indole ring. Second, by dint of proximity, the peptide bond is the most important quencher of tryptophan fluorescence in peptides and proteins. Simply permuting the position of tryptophan in our series of peptides, which lack quenching side chains, changes the fluorescence quantum yield by a factor of six. Third, the effect of backbone conformation on tryptophan fluorescence is manifest in two ways: amplitude or χ_1 rotamer population and lifetime.

SUPPLEMENTARY MATERIAL

An online supplement to this article can be found by visiting BJ Online at http://www.biophysj.org.

We thank Dr. Dale Ray for assistance with NMR spectroscopy and Professor Frank D. Sönnichsen for helpful discussions about peptide structure determination.

REFERENCES

Ababou, A., and E. Bombarda. 2001. On the involvement of electron transfer reactions in the fluorescence decay kinetics heterogeneity of proteins. *Protein Sci.* 10:2102–2113.

Adams, P. D., Y. Chen, K. Ma, M. G. Zagorski, F. D. Sönnichsen, M. L. McLaughlin, and M. D. Barkley. 2002. Intramolecular quenching of tryptophan fluorescence by the peptide bond in cyclic hexapeptides. *J. Am. Chem. Soc.* 124:9278–9286.

Bax, A., and D. G. Davis. 1985. MLEV-17-based two-dimensional homonuclear magnetization transfer spectroscopy. *J. Magn. Reson.* 65: 355–360.

Beechem, J. M. 1989. A second generation global analysis program for the recovery of complex inhomogeneous fluorescence decay kinetics. *Chem. Phys. Lipids.* 50:237–251.

Beratan, D. N., J. N. Betts, and J. N. Onuchic. 1992. Tunneling pathway and redox-state-dependent electronic couplings at nearly fixed distance in electron-transfer proteins. *J. Phys. Chem.* 96:2852–2855.

Callis, P. R. 1997. ^1L_a and ^1L_b Transitions of tryptophan: applications of theory and experimental observations to fluorescence of proteins. *Met. Enzymol.* 278:113–151.

Callis, P. R., and B. K. Burgess. 1997. Tryptophan fluorescence shifts in proteins from hybrid simulations: an electrostatic approach. *J. Phys. Chem. B.* 101:9429–9432.

Callis, P. R., and J. T. Vivian. 2003. Understanding the variable fluorescence quantum yield of tryptophan in proteins using QM–MM simulations. Quenching by charge transfer to the peptide backbone. *Chem. Phys. Lett.* 369:409–414.

Chen, R. F. 1967. Fluorescence quantum yields of tryptophan and tyrosine. *Anal. Lett.* 1:35–42.

Chen, R. F., J. R. Knutson, H. Ziffer, and D. Porter. 1991. Fluorescence of tryptophan dipeptides: correlations with the rotamer model. *Biochemistry.* 30:5184–5195.

Chen, Y., and M. D. Barkley. 1998. Toward understanding tryptophan fluorescence in proteins. *Biochemistry.* 37:9976–9982.

Chen, Y., B. Liu, H.-T. Yu, and M. D. Barkley. 1996. The peptide bond quenches indole fluorescence. *J. Am. Chem. Soc.* 118:9271–9278.

Clayton, A. H., and W. H. Sawyer. 1999. Tryptophan rotamer distributions in amphipathic peptides at a lipid surface. *Biophys. J.* 76:3235–3242.

Dahms, T. E. S., K. J. Willis, and A. G. Szabo. 1995. Conformational heterogeneity of tryptophan in a protein crystal. *J. Am. Chem. Soc.* 117:2321–2326.

Donzel, B., P. Gaudchon, and P. Wahl. 1974. Study of the conformation in the excited state of two tryptophanyl diketopiperazines. *J. Am. Chem. Soc.* 96:801–808.

Dunbrack, R. L., Jr., and M. Karplus. 1993. Backbone-dependent rotamer library for proteins. Application to side-chain prediction. *J. Mol. Biol.* 230:543–574.

Dunbrack, R. L., Jr., and M. Karplus. 1994. Conformational analysis of the backbone-dependent rotamer preferences of protein sidechains. *Nat. Struct. Biol.* 1:334–340.

Gordon, H. L., H. C. Jarrell, A. G. Szabo, K. J. Willis, and R. L. Somorjai. 1992. Molecular-dynamics simulations of the conformational dynamics of tryptophan. *J. Phys. Chem.* 96:1915–1921.

Havel, T. F., I. D. Kuntz, and G. M. Crippen. 1983. The combinatorial distance geometry method for the calculation of molecular conformation. I. A new approach to an old problem. *J. Theor. Biol.* 104:359–381.

Hellings, M., M. De Maeyer, S. Verheyden, Q. Hao, E. J. M. Van Damme, W. J. Peumans, and Y. Engelborghs. 2003. The dead-end elimination method, tryptophan rotamers, and fluorescence lifetimes. *Biophys. J.* 85: 1894–1902.

Hopfield, J. J. 1974. Electron transfer between biological molecules by thermally activated tunneling. *Proc. Natl. Acad. Sci. USA.* 71: 3640–3644.

Hudson, B. S., J. M. Huston, and G. Soto-Campos. 1999. A reversible ''dark state'' mechanism for complexity of the fluorescence of tryptophan in proteins. *J. Phys. Chem. A.* 103:2227–2234.

Kessler, H., U. Anders, and M. Schudok. 1990. An unexpected *cis* peptide bond in the minor conformation of a cyclic hexapeptide containing only secondary amide bonds. *J. Am. Chem. Soc.* 112:5908–5916.

Kessler, H., J. W. Bats, C. Griesinger, S. Koll, M. Will, and K. Wagner. 1988a. Peptide conformations. 46. Conformational analysis of a super-potent cytoprotective cyclic somatostatin analog. *J. Am. Chem. Soc.* 110:1033–1049.

Kessler, H., M. Klein, and K. Wagner. 1988b. Peptide conformation. 48. Conformation and biological activity of proline containing cyclic retro-analogues of somatostatin. *Int. J. Pept. Protein Res.* 31:481–498.

Kumar, A., R. R. Ernst, and K. Wüthrich. 1980. A two-dimensional nuclear Overhauser enhancement (two-dimensional NOE) experiment for the elucidation of complete proton-proton cross-relaxation networks in biological macromolecules. *Biochem. Biophys. Res. Commun.* 95:1–6.

Laboulais, C., E. Deprez, H. Leh, J.-F. Mouscadet, J.-C. Brochon, and M. Le Bret. 2001. HIV-1 integrase catalytic core: molecular dynamics and simulated fluorescence decays. *Biophys. J.* 81:473–489.

Ladokhin, A. S. 1999. Red-edge excitation study of nonexponential fluorescence decay of indole in solution and in a protein. *J. Fluoresc.* 9:1–9.

Lakowicz, J. R. 2000. On spectral relaxation in proteins. *Photochem. Photobiol.* 72:421–437.

Larsen, O. F. A., I. H. M. van Stokkum, A. Pandit, R. van Grondelle, and H. van Amerongen. 2003. Ultrafast polarized fluorescence measurements on tryptophan and a tryptophan-containing peptide. *J. Phys. Chem. B.* 107:3080–3085.

Marcus, R. A., and N. Sutin. 1985. Electron transfers in chemistry and biology. *Biochim. Biophys. Acta.* 811:265–322.

McLendon, G. 1988. Long-distance electron transfer in proteins and model systems. *Acc. Chem. Res.* 21:160–167.

McMahon, L. P., W. J. Colucci, M. L. McLaughlin, and M. D. Barkley. 1992. Deuterium isotope effects in constrained tryptophan derivatives: implications for tryptophan photophysics. *J. Am. Chem. Soc.* 114:8442–8448.

Moncrieffe, M. C., N. Juranic, M. D. Kemple, J. D. Potter, S. Macura, and F. G. Prendergast. 2000. Structure-fluorescence correlations in a single tryptophan mutant of carp parvalbumin: solution structure, backbone and side-chain dynamics. *J. Mol. Biol.* 297:147–163.

Nanda, V., and L. Brand. 2000. Aromatic interactions in homeodomains contribute to the low quantum yield of a conserved, buried tryptophan. *Proteins Struct. Funct. Genet.* 40:112–125.

Nishino, N., M. Xu, H. Mihara, T. Fujimoto, Y. Ueno, and H. Kumagai. 1992. Sequence dependence in solid-phase synthesis cyclization-cleavage for cyclo(arginyl-glycyl-aspartyl-phenylglycyl). *Tetrahedron Lett.* 33:1479–1482.

Pachler, K. G. R. 1963. Nuclear magnetic resonance (NMR) study of some α-amino acids. I. Coupling constants in alkaline and acidic medium. *Spectrochim. Acta.* 19:2085–2092.

Pandit, A., O. F. A. Larsen, I. H. M. van Stokkum, R. van Grondelle, R. Kraayenhof, and H. van Amerongen. 2003. Ultrafast polarized fluorescence measurements on monomeric and self-associated melittin. *J. Phys. Chem. B.* 107:3086–3090.

Petrich, J. W., M. C. Chang, D. B. McDonald, and G. R. Fleming. 1983. On the origin of nonexponential fluorescence decay in tryptophan and its derivatives. *J. Am. Chem. Soc.* 105:3824–3832.

Piotto, M., V. Saudek, and V. Sklenar. 1992. Gradient-tailored excitation for single-quantum NMR spectroscopy of aqueous solutions. *J. Biomol. NMR.* 2:661–665.

Robbins, R. J., G. R. Fleming, G. S. Beddard, G. W. Robinson, P. J. Thistlewhaite, and G. J. Woolfe. 1980. Photophysics of aqueous tryptophan: pH and temperature effects. *J. Am. Chem. Soc.* 102:6271–6279.

Ross, J. B. A., K. W. Rousslang, and L. Brand. 1981. Time-resolved fluorescence and anisotropy decay of tryptophan in adrenocorticotropin-(1–24). *Biochemistry.* 20:4361–4369.

Ross, J. B. A., H. R. Wyssbrod, R. A. Porter, G. P. Schwartz, C. A. Michaels, and W. R. Laws. 1992. Correlation of tryptophan fluorescence intensity decay parameters with ^{1}H NMR-determined rotamer conformations: [tryptophan^2]oxytocin. *Biochemistry.* 31:1585–1594.

Saito, I., H. Sugiyama, A. Yamamoto, S. Muramatsu, and T. Matsuura. 1984. Photoinduced reactions. 158. Photochemical hydrogen-deuterium exchange reaction of tryptophan. The role of nonradiative decay of singlet tryptophan. *J. Am. Chem. Soc.* 106:4286–4287.

Shen, X., and J. R. Knutson. 2001. Subpicosecond fluorescence spectra of tryptophan in water. *J. Phys. Chem. B.* 105:6260–6265.

Shizuka, H., M. Serizawa, T. Shimo, I. Saito, and T. Matsuura. 1988. Fluorescence-quenching mechanism of tryptophan. Remarkably efficient internal proton-induced quenching and charge-transfer quenching. *J. Am. Chem. Soc.* 110:1930–1934.

Sillen, A., J. F. Diaz, and Y. Engelborghs. 2000. A step toward the prediction of the fluorescence lifetimes of tryptophan residues in proteins based on structural and spectral data. *Protein Sci.* 9:158–169.

Smallcombe, S. H., S. L. Patt, and P. A. Keifer. 1995. WET solvent suppression and its applications to LC NMR and high-resolution NMR spectroscopy. *J. Magn. Reson. A.* 117:295–303.

Szabo, A. G., and D. M. Rayner. 1980. Fluorescence decay of tryptophan conformers in aqueous solution. *J. Am. Chem. Soc.* 102:554–563.

Vander Donckt, E. 1969. Fluorescence solvent shifts and singlet excited state pKs of indole derivatives. *Bull. Soc. Chim. Belg.* 78:69–75.

Vivian, J. T., and P. R. Callis. 2001. Mechanisms of tryptophan fluorescence shifts in proteins. *Biophys. J.* 80:2093–2109.

Volkert, W. A., R. R. Kuntz, C. A. Ghiron, R. F. Evans, R. Santus, and M. Bazin. 1977. Flash photolysis of tryptophan and *N*-acetyl-L-tryptophanamide: the effect of bromide on transient yields. *Photochem. Photobiol.* 26:3–9.

Willis, K. J., W. Neugebauer, M. Sikorska, and A. G. Szabo. 1994. Probing α-helical secondary structure at a specific site in model peptides via restriction of tryptophan side-chain rotamer conformation. *Biophys. J.* 66:1623–1630.

Wuthrich, K. 1986. NMR of Proteins and Nucleic Acids. American Chemical Society, Boca Raton, FL.

Yu, H. T., W. J. Colucci, M. L. McLaughlin, and M. D. Barkley. 1992. Fluorescence quenching in indoles by excited-state proton transfer. *J. Am. Chem. Soc.* 114:8449–8454.

Zawadzki, K. M., C.-P. Pan, M. D. Barkley, D. Johnson, and S. S. Taylor. 2003. Endogenous tryptophan residues of cAPK regulatory subunit type IIβ reveal local variations in environments and dynamics. *Proteins Struct. Funct. Genet.* 51:552–561.